Journal of Sound and Vibration (2002) **258**(1), 179–190
doi:10.1006/jsvi.5039, available online at http://www.idealibrary.com on IDEAL®

LETTERS TO THE EDITOR

ENERGY EFFICIENT ACTUATORS IN VIBRATION CONTROL OF PLATED STRUCTURES

A. Mukherjee and S. Joshi

Department of Civil Engineering, Indian Institute of Technology, Bombay, Mumbai 400 076, *India.*
E-mail: abhijit@civil.iitb.ac.in

(*Received* 16 *November* 2001, *and in final form* 14 *February* 2002)

1. INTRODUCTION

Piezoelectric materials are popularly used as energy transducers in several structural applications such as shape control, vibration suppression, acoustic control, etc. When used as actuators in vibration control, these materials convert electrical energy into mechanical energy to generate the control forces. In such an application, a critical issue that needs to be considered is the electrical energy that the actuators consume in order to produce the desired response. It is highly desirable to minimize the total energy consumption of the actuators, as in many practical situations only limited power may be available. The knowledge of energy consumption is also necessary to design the driving electronics for the active vibration control. One of the ways of achieving efficiency is using optimal actuator configurations. The present work investigates the energy consumption characteristics of a modal actuator for a cantilever plate.

Modal sensing and actuation has been a topic of interest in recent years. Reference [1] contains a summary of modal sensing and actuation techniques. One of the ways of designing modal actuators is by spatially weighting the electrode surface in terms of geometry and poling. Modal actuators combined with modal sensors improve the control characteristics as they minimize the spillover effects and alleviate the need for exhaustive signal processing. Lee and Moon [2] developed a theory to derive modal sensors and actuators for one-dimensional structures using modal equations. Friswell [3] used finite element shape functions to design modal sensors and actuators for Euler–Bernoulli beams. Mukherjee and Joshi [4] presented a gradientless shape design procedure to obtain spatially optimized transducers for shape control of piezolaminated plates.

Few researchers have addressed the issue of power and energy consumption of piezoelectric actuators in exciting the structures. Jordan *et al.* [5] developed empirical relations for predicting power consumption characteristics of a PZT actuator. Brennan and McGowan [6] showed that for a completely damped structure, the power requirement of a piezoelectric actuator depends only on the geometry and material properties of the structure, and the driving voltage and frequency of the control signal. Liang *et al.* [7] determined the optimal actuator configuration based on actuator power factor. The actuator power factor was defined as the ratio of dissipative mechanical power to the supplied electrical power. Stein *et al.* [8] used an electromechanical impedance approach to determine the power consumption of piezoelectric actuators driving a simply supported

0022-460X/02/$35.00

beam in a fluid medium. Mukherjee and Joshi [9] presented an iterative technique to determine actuator profiles that minimize power consumption in obtaining the desired displacements in the structure. The algorithm was based on the work done by the actuators on the host structure. In the present work, the concept is extended to the dynamic control of the structure. The main challenge in the dynamic control with shaped actuators is to determine the profile of the actuator for a deformed shape that varies with time. A simple solution to this problem is to design the actuator profile for the fundamental mode shape. Such an actuator excites only that mode that it is designed for and therefore, it can be called as the modal actuator. The participation of the fundamental mode is most dominant in a vibrating structure. Therefore, an actuator shaped for the fundamental mode should also be most efficient in controlling the vibrating structure.

The efficacy of a modal actuator in energy consumption is investigated. The actuator design obtained from the technique developed by the authors is examined. A long cantilever plate is considered as a demonstration model and the mode-1 actuator is employed in controlling the response of the plate. The response of the modal actuator is compared with that of the *unweighted* actuator. It is found that the modal actuator is more energy efficient than the unweighted actuator.

2. MATHEMATICAL FORMULATION

The equations of motion for a structure subjected to time-dependent forces can be written as a set of second order differential equations in the following form:

$$\mathbf{M}\ddot{\boldsymbol{\delta}} + \mathbf{C}\dot{\boldsymbol{\delta}} + \mathbf{K}\boldsymbol{\delta} = \mathbf{F}(\mathbf{t}) \tag{1}$$

where **M**, **C** and **K** are the mass, damping and stiffness matrices of the system, $\ddot{\boldsymbol{\delta}}, \dot{\boldsymbol{\delta}}$ and $\boldsymbol{\delta}$ are the acceleration, velocity and displacement vectors respectively. The force vector **F(t)** comprises the vectorial sum of external time-dependent forces and the control forces. In the present work, an eight-node plate finite element with five degrees of freedom per node (u, v, w, θ_x and θ_y) is employed. The detailed formulation for the mass, stiffness and the damping matrices can be found elsewhere [10]. A brief explanation on the formulation of the force vector is presented here.

2.1. FORCE VECTOR

The force vector comprises two parts, namely, the externally applied time-dependent forces and the time-dependent actuator forces generated by the piezoelectric actuators. The sensors in the system sense the signal due to externally applied forces. The signal is fed back to the actuator that generates the control forces. In this section, the formulation of the sensor and actuator mechanics is discussed in brief.

2.2. SENSOR MECHANICS

According to the Gauss law, the closed circuit charge (q) measured through the electrodes of a sensor patch in kth layer is

$$q = \frac{1}{2}\left(\left[\int_R D_3^k \, \mathrm{d}A\right]_{z=z_k} + \left[\int_R D_3^k \, \mathrm{d}A\right]_{z=z_{k-1}}\right). \tag{2}$$

In finite element terms:

$$q = \int_R (\mathbf{e}B\boldsymbol{\delta}_e)\,\mathrm{d}A. \tag{3}$$

In equations (2) and (3), $\mathbf{D}^k$ corresponds to the electric field displacement vector, $\mathbf{e}$ is the matrix of piezoelectric constants, $\mathbf{B}$ is the strain–displacement matrix and δ_e is the deformation vector. The sensed voltage (Vs) is

$$V_s = q/C \tag{4}$$

where C is the capacitance of the piezoelectric material.

2.3. ACTUATOR MECHANICS

The electric field vector is assumed to act across the thickness of the plate so that the electric field intensity is calculated as

$$(E_3)^k = \frac{V^k}{h^k} \tag{5}$$

where the subscript 3 refers to the z direction, h^k is the thickness of the kth layer and V^k the voltage across the kth layer. The equivalent actuator forces (N_x^p, N_y^p and N_{xy}^p) and moments (M_x^p, M_y^p and M_{xy}^p) are given by

$$\begin{Bmatrix} N_x^{\mathrm{p}} & M_x^{\mathrm{p}} \\ N_y^{\mathrm{p}} & M_y^{\mathrm{p}} \\ N_{xy}^{\mathrm{p}} & M_{xy}^{\mathrm{p}} \end{Bmatrix} = \sum_{k=1}^{Nlay} \int_{z(k-1)}^{z(k)} \begin{Bmatrix} e_{31} \\ e_{32} \\ 0 \end{Bmatrix}^k (1, z)(E_3)^k\,\mathrm{d}z. \tag{6}$$

The nodal force vector is given as by

$$F^{\mathrm{p}} = \int B^{\mathrm{T}} \begin{Bmatrix} N^{\mathrm{p}} \\ M^{\mathrm{p}} \end{Bmatrix} \mathrm{d}A. \tag{7}$$

3. CONTROL ALGORITHM

A velocity feedback algorithm is employed in the present work. The charge (q) developed on the sensor is differentiated with respect to time to obtain the current. The current is amplified using a current amplifier and fed back to the actuators. The control forces generated by the actuators contribute to the velocity terms of equation (1). Therefore, the damping characteristics of the system are altered.

The sensor voltage is calculated as

$$V_s = \frac{\mathrm{d}q}{\mathrm{d}t} R \tag{8}$$

where R is the resistance of the piezoelectric material. The feedback voltage is

$$V_a = G_i V_s = G\frac{\mathrm{d}q}{\mathrm{d}t} \tag{9}$$

where G_i is the current amplifier gain and G is a combined coefficient representing the gain and the resistance of the piezoelectric material.

4. ENERGY CONSUMPTION

The apparent electrical power consumed by the piezoelectric actuator is given by

$$P = V_a I \tag{10}$$

where V_a is the actuator input voltage and I is the current. As power is the time rate of energy, the cumulative apparent electrical energy consumed (E_c) is given by

$$E_c = \int_T P \, \Delta t. \tag{11}$$

The apparent electrical energy is the total electrical energy supplied to the system. In the present context, we define the cumulative apparent electrical energy in terms of an energy parameter (E_p) given by

$$E_p = \sum k V_a^2 \, \Delta t \tag{12}$$

where k is the coefficient that accounts for the actuator area and the resistance and Δt is the time step.

5. TRANSDUCER SHAPE DESIGN

In this section, an iterative algorithm is presented for adaptive design of transducer profiles. It is to be noted that a reciprocal relationship exists between a sensor and an actuator. Therefore, the shape of the actuator that excites a particular mode (modal actuator) is also the shape of the sensor that responds only to that mode (modal sensor). The present iterative procedure can, therefore, be employed in designing both modal sensors and actuators. The objective is to minimize the quadratic measure of the residual deviation of the current deformations of the structure from its desired state. The objective function is thus defined by

$$min\left[\int \{\boldsymbol{\delta}_i(p_1, A_1, \ldots, p_n, A_n) - \boldsymbol{\delta}_0\}^2 \, \mathrm{d}A\right] \tag{13}$$

where $\boldsymbol{\delta}_i$ is the normalized deformation vector in ith iteration, ($A_i, \ldots, A_n$) are the areas of actuators that are switched on, ($p_1, \ldots, p_n$) are the actuator position vectors and $\boldsymbol{\delta}_0$ is the normalized desired deformation vector.

The step-by-step procedure for actuator design is described below:

(1) The structure is discretized into a fine finite element mesh.

(2) The shape design process begins with a maximal *seed* design wherein all the actuators are switched on. The mode shape for which the actuator profile is to be obtained is the deformation vector. Using sensor relation, the voltage in each element (V_s^e) is calculated.

To begin the process of removal of the actuators, a concept of *front opening* is introduced (Figure 1(a)). The front is initially defined by the physical boundaries of the structure. The actuators that lie on the front are removed from the locations of minimal absolute curvature. Only those actuators that surround the front are the candidates for state change (Figure 1(b)). The front progresses in both directions and the actuator gradually adapts to the shape that is most efficient in obtaining the desired structural configuration. The front opening and subsequent removal of the actuators surrounding the front ensures that the final design that emerges is smooth and eliminates formation of such voids that could render its practical implementation difficult.

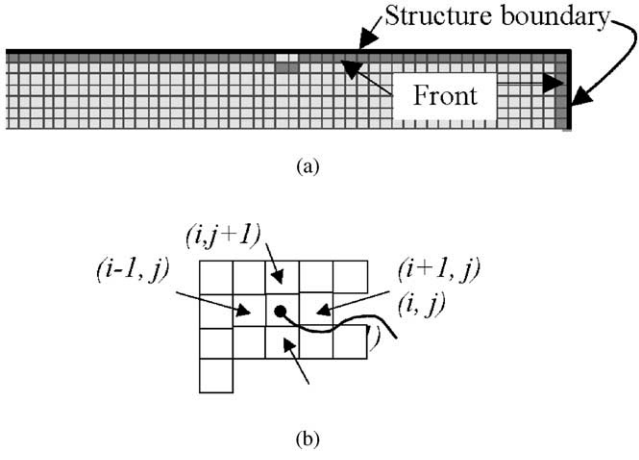

Figure 1. Front growth: (a) Front opening. (b) Actuator adjacency.

(3) The structure is analyzed based on the current actuator configuration under unit voltage and the voltages developed due to current actuator configuration are calculated (V_a^e).

(4) The voltages V_a^e and V_s^e are normalized with respect to their maximum values.

$$\bar{V}_s^e = \frac{V_s^e}{(V_s^e)_{\max}}, \qquad \bar{V}_a^e = \frac{V_a^e}{(V_a^e)_{\max}}. \tag{14}$$

The residual voltages (V_r^e) for the elements on the front are determined by

$$V_r^e = (\bar{V}_s^e - \bar{V}_a^e). \tag{15}$$

The elements that have negative residuals are potential actuators which are to be removed. In practice, a predetermined fraction of these actuators are removed.

(5) The quadratic measure of the global residual deviation (α) in deformation is calculated as

$$\alpha = \sum_{i=1}^{ndof} (\boldsymbol{\delta}_i - \boldsymbol{\delta}_0)^2. \tag{16}$$

(6) Steps 3–5 are repeated till the value of α is acceptably small.

6. NUMERICAL EXAMPLE

6.1. A LONG CANTILEVER PLATE SUBJECTED TO AIR BLAST

In this example, the response of a cantilever aluminum plate (100 mm × 20 mm × 1 mm), subjected to blast pressure applied over the surface of the plate, is investigated (Figure 2). Due to symmetry only half the plate is modelled using a 75×7 finite element mesh. The constituent properties of the plate are given in Table 1. First four bending modes (Table 2) are included in the transient analysis. Two PZT layers are attached (Table 1), one each at top and bottom, to control the response of the plate. Velocity feedback algorithm discussed in section 3 is employed in controlling the response of the plate.

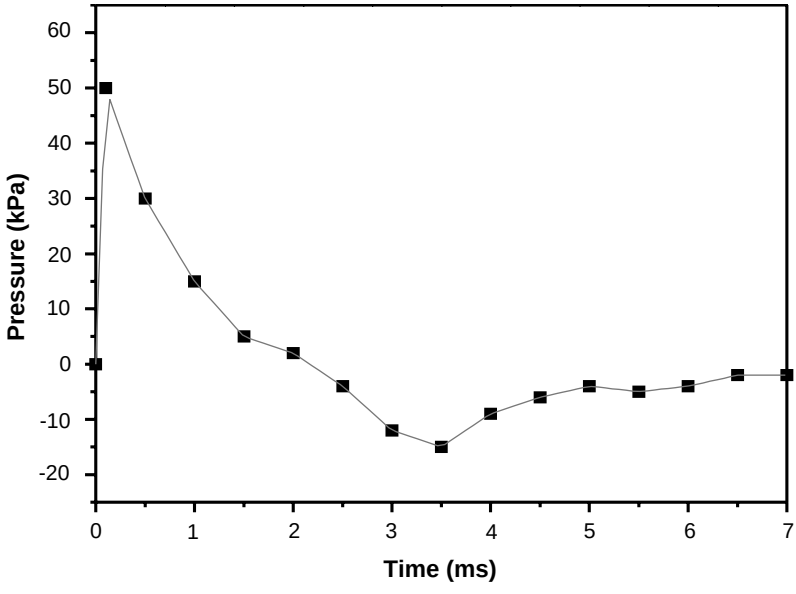

Figure 2. Air blast (reference [11]).

TABLE 1

Constituent properties

Properties	Aluminum	PZT
Elastic modulus ($E_{11} = E_{22}$) (GPa)	70·0	63·0
Shear modulus (GPa)	28·0	24·2
Poisson ratio, ν	0·30	0·30
Density ρ ($\mathrm{N\,s^2/m^4}$)	2700	7600
Thickness t (mm)	1	0·25
Piezoelectric constants ($d_{31} = d_{32}$) (C/N)	—	-256×10^{-12}
Dielectric coefficients $\bar{\varepsilon}_{33}$ (F/m)	—	$1{\cdot}151 \times 10^{-9}$

TABLE 2

Natural frequencies (Hz)

Mode no.	Mode 1	Mode 2	Mode 3	Mode 4
Frequency	98·41	616·01	1721·51	3364·00

6.2. EFFECT OF ACTUATOR SHAPES

In this section, the influence of the shape of the actuator on the response of the structure is investigated. The shapes considered are the actuator covering the entire surface of the structure (unweighted actuator) and the actuator shaped to excite the fundamental mode of the structure (Figure 3). The shape of the actuator for the fundamental mode has been

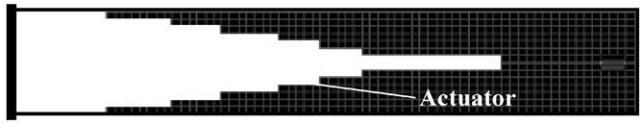

Figure 3. Actuator shape optimized for the fundamental mode of the cantilever plate.

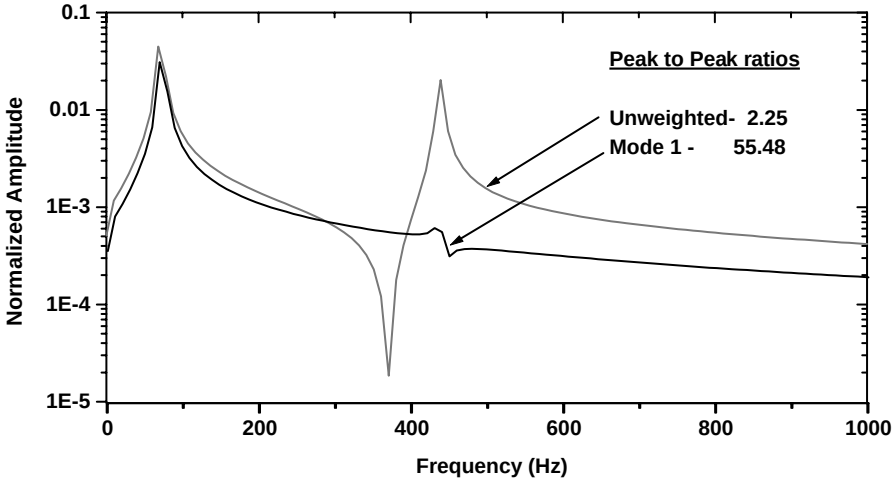

Figure 4. Frequency response of the modal actuator and the unweighted actuator to electrical excitation.

obtained from the technique described in section 5. To examine the validity of the design, both actuator shapes are excited using sinusoidal voltage of the nature $V = V_0$ $(\sin \omega_1 t + \sin \omega_2 t)$, where ω_1 and ω_2 are the forcing frequencies close to the first two natural frequencies of the system. The modal actuator primarily excites the fundamental mode of the structure whereas the unweighted actuator excites both the modes (Figure 4). Thus, the modal actuator design obtained using the optimization technique is validated. This modal actuator design is further used in controlling the response of the plate subjected to blast load. The vibration control and the energy consumption characteristics of the modal actuator are studied vis-à-vis a conventional unweighted actuator.

Figure 5 shows that for the same damping ratio ($\xi = 0{\cdot}002$) and gain ($G = 2{\cdot}0 \times 10^6$), the attenuation rate using modal actuator is marginally lower than that of the unweighted actuator. However, a more relevant comparison could be between the energy consumption characteristics of these actuator profiles. It is seen from Figure 6 that the energy consumed by the modal actuator (curve 2) is almost half of that consumed by the unweighted actuator (curve 1). This is an important observation as in many practical situations only limited energy may be available and it is desirable to use as less energy as possible in suppressing vibration.

As the gain is increased to $4{\cdot}0 \times 10^6$, a marked difference in the response is observed for unweighted and modal actuators. The unweighted actuator leads to system instability as the response amplifies instead of attenuating. This is characterized by a sharp increase in the energy consumption (Figure 6, curve 3). However, with the modal actuator the

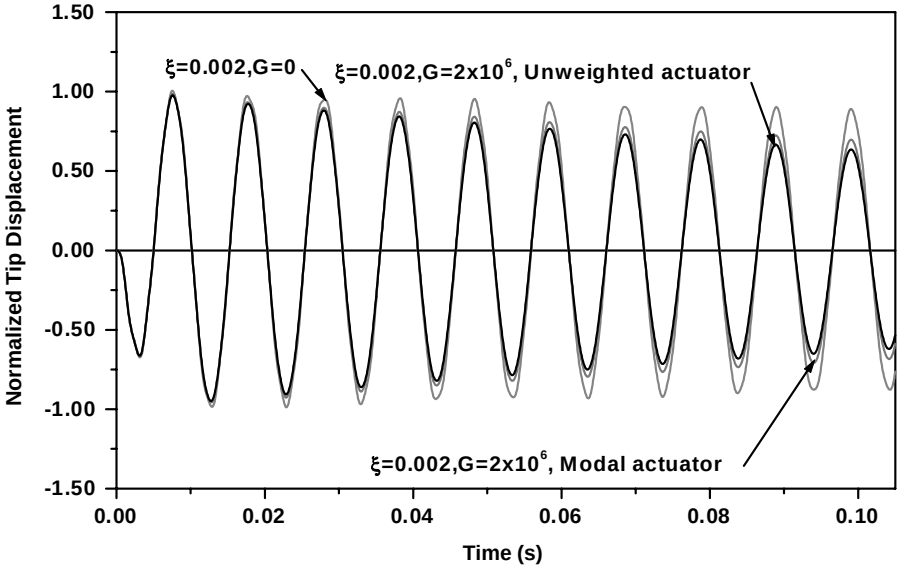

Figure 5. Normalized tip displacement response with unweighted and modal actuator.

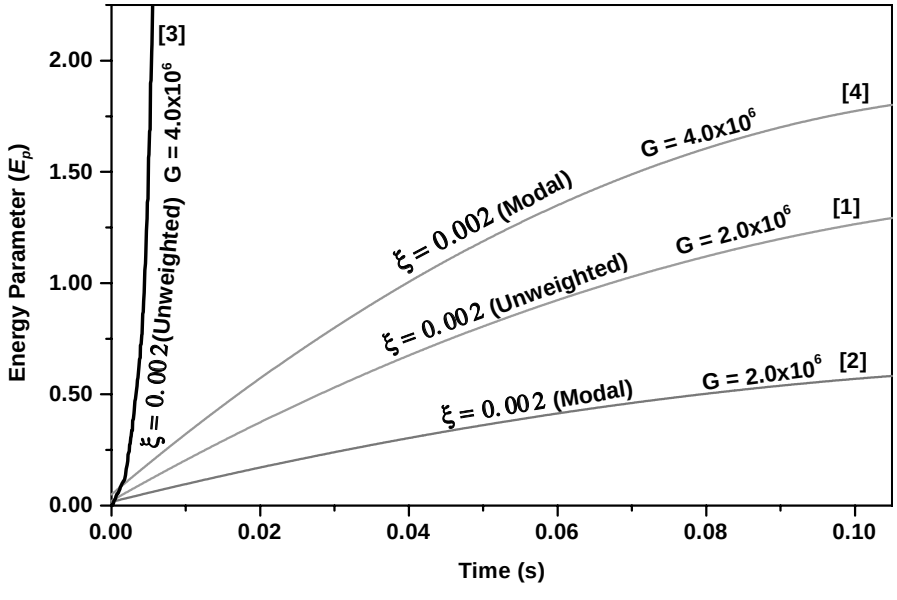

Figure 6. Energy characteristics of unweighted and modal actuators for various gains.

response attenuates and curve 4 shows a stabilizing effect. The tip deflections of the plate due to the unweighted and the modal actuators are presented in Figure 7. While the unweighted actuator leads to amplification of deflection, the modal actuator remains stable and it produces a steady response. Thus, the modal actuator displays improved characteristics as it allows faster vibration suppression as compared to the unweighted actuator. It is to be noted that there is also an upper limit to the gain that can be used for

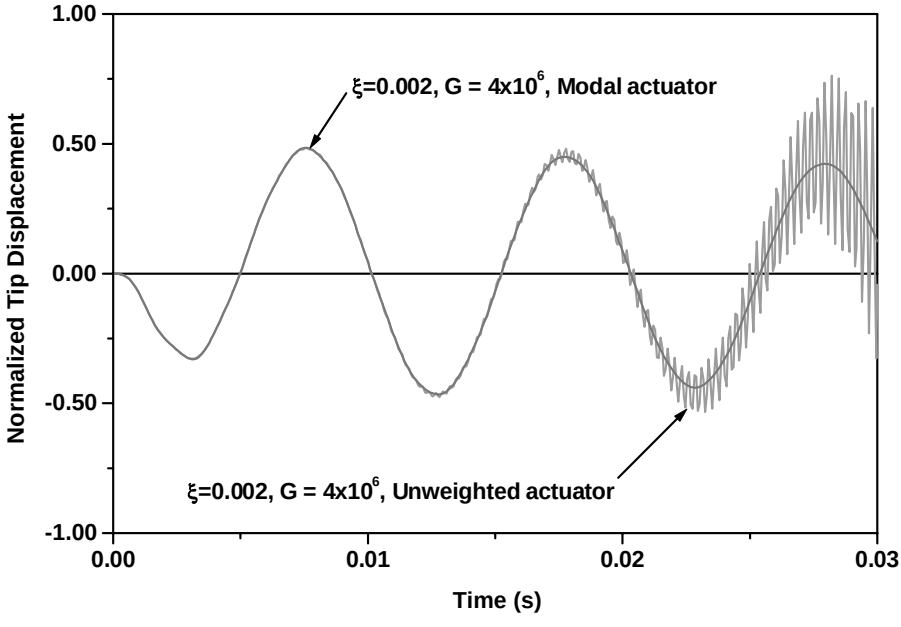

Figure 7. Tip displacement response using unweighted and modal actuators.

the modal actuator beyond which the response becomes unstable. However, that limit for the modal actuator is much higher than that for the unweighted actuator. It can be shown that for piezoelectric layers bonded symmetrically to the top and the bottom of the plate, the limiting gain for an actuator is inversely proportional to the actuator area. The limiting gain can be written as

$$G_{lim} = \frac{K}{\int_L b_x \, \mathrm{d}x} \tag{17}$$

where K is a factor depending on the bending stiffness and the piezoelectric properties of the structure and b_x is the width of the actuator at a distance x from the origin. For a one-dimensional plate, the value of K is given by

$$K = \frac{2\bar{D}}{e_{31}^2(T+h)} \tag{18}$$

where $\bar{D}$ is the flexural rigidity of the plate per unit width, e_{31} is the piezoelectric coefficient in the x direction, T is the thickness of the plate and h is the thickness of the piezoelectric layer.

It can be seen that as the shaped actuator covers much less area as compared to the unweighted actuator, the limiting gain for the shaped actuator is higher than that of the unweighted actuator. For the present cantilever example, the modal actuator area covers about one-third plate area as compared to the unweighted actuator and therefore the limiting gain is approximately three times that of the unweighted actuator.

The efficacy of the modal actuator over unweighted actuator is further examined with the following objectives:

1. Energy consumption for the same attenuation rate as that for the unweighted actuator.
2. Attenuation rate for same energy characteristics as that for the unweighted actuator.

The displacement response and the energy consumption curve for unweighted actuator at 0·2% material damping and $G = 2 \times 10^6$ are set as the benchmark for comparing the response of the modal actuator. In the first case, the objective is to find out a constant gain at which the modal actuator simulates the response of the unweighted actuator as closely as possible. To obtain this value, the maximum energies consumed by the unweighted actuator and the modal actuator at $G = 2 \times 10^6$ are equated as we expect the energy curve to lie between these two curves. Thus,

$$G_2 = \left[\sqrt{\frac{k_1}{k_2}}\left(\frac{V_1}{V_2}\right)\right] G_1 \tag{19}$$

where G_1 is the gain in unweighted actuator, G_2 the gain in modal actuator, k_1 the coefficient accounting for area and resistance for the unweighted actuator, k_2 the coefficient accounting for the area and the resistance of the modal actuator, V_1 the sensed voltage in the case of the unweighted actuator at the final time step, and V_2 the sensed voltage in the case of the modal actuator at the final time step.

In the present case, equation (20) gives the value of $G_2 = 3{\cdot}0 \times 10^6$. The energy curves in Figure 8 show that the energy consumed by the modal actuator for the same attenuation rate is lower (curve 3) than that of the unweighted actuator (curve 1) and the difference is about 11%. Thus, the modal actuator is more energy efficient at this gain as compared to the unweighted actuator.

In the second case, the gain is varied such that the cumulative energy consumed by the modal actuator at each time step is the same as in the case of the unweighted actuator. Equating the energies in the unweighted and modal actuator at each time step, the gain at each time step is given as

$$G_{si} = \left[\frac{\sum V_{fi}\sqrt{k_f}}{\sum V_{si}\sqrt{k_s}}\right] G_f \tag{20}$$

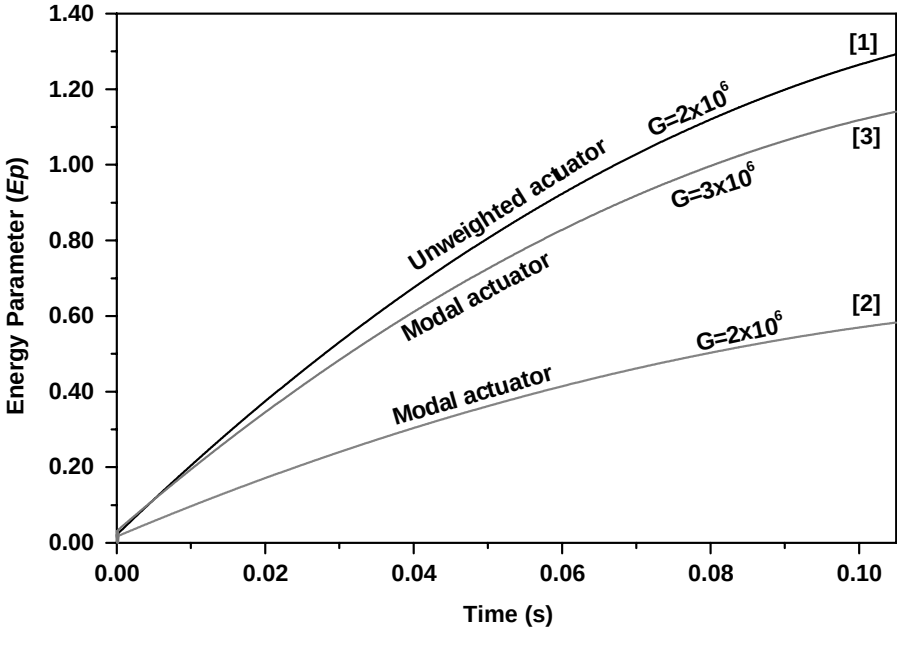

Figure 8. Cumulative energy consumption for unweighted and modal actuators for different gains.

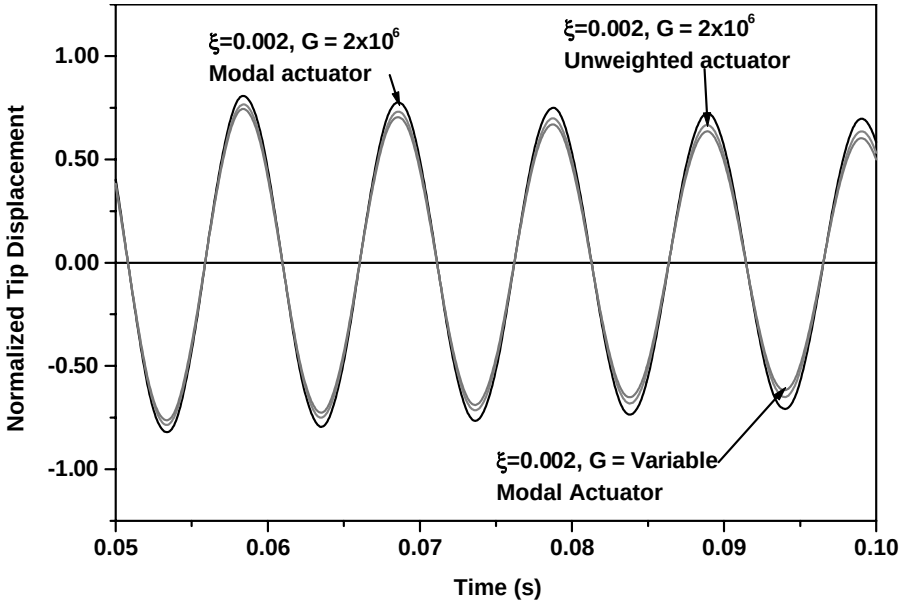

Figure 9. Comparison of the tip displacement responses using unweighted and modal actuators at different gains.

where G_{si} is the gain in modal actuator at ith time step, G_f the gain in unweighted actuator, k_s the coefficient accounting for the area and the resistance of modal actuator, k_f the coefficient accounting for the area and the resistance for the unweighted actuator, V_{si} the sensed voltage in the case of the modal actuator at ith time step, and V_{fi} the sensed voltage in the case of the unweighted actuator at ith time step.

As seen in Figure 9, the modal actuator with variable gain shows improved response attenuation rate. The damping ratio in this case is about 12% higher than the unweighted actuator with constant gain. Thus, for the same energy consumption, the modal actuator with variable gain is a better performer than the unweighted actuator with constant gain.

REFERENCES

1. M. L. Fripp and M. J. Atalla 2001 *The Shock and Vibration Digest* **33**, 1, 3–14. Review of modal sensing and actuation techniques.
2. C.-K. Lee and F. C. Moon 1990 *American Society of Mechanical Engineers Journal of Applied Mechanics* **57**, 434–441. Modal sensors/actuators.
3. M. I. Friswell 2001 *Journal of Sound and Vibration* **241**, 361–372. On the design of modal actuators and sensors.
4. A. Mukherjee and S. P. Joshi 2001 *First Asian–Pacific Congress on Computational Mechanics (APCOM'01)*, Sydney, November 19–23, 2001, 1413–1417. Actuator shape optimization for control of smart laminated plates.
5. T. Jordan, Z. Ounaies, J. Tripp and P. Tcheng 2000 *NASA/CR*-2000-209861. Electrical properties and power considerations of a piezoelectric actuator.
6. M. C. Brennan and A.-M. McGowan 1997 *Proceedings of SPIE: Smart Structures and Materials* **3039**, 660–664. Piezoelectric power requirements for active vibration control.
7. C. Liang, F. P. Sun and C. A. Rogers 1995 *Journal of Intelligent Material System and Structures* **6**, 456–464. Determination of design of optimal actuator location and configuration based on actuator power factor.

8. S. C. Stein, C. Liang and C. A. Rogers 1994 *Journal of Acoustical Society of America* **96**, 1598–1604. Power consumption of piezoelectric actuators driving a simply supported beam considering fluid coupling.
9. A. Mukherjee and S. P. Joshi 2001 *Smart Materials and Structures* **10**, 305–313. Design of actuator profiles for minimum power consumption.
10. A. Mukherjee 1987 *Ph.D. Thesis, Indian Institute of Technology, Kharagpur*. On finite element dynamic and stability analyses of stiffened plated structures.
11. R. Houlston, J. E. Slater, N. Pegg and G. G. Des Rochers 1985 *Computers and Structures* **21**, 273–289. On analysis of structural response of ship panels subjected to air blast loading.